JBC RESEARCH ARTICLE

Loss of the ceramide synthase HYL-2 from *Caenorhabditis elegans* impairs stress responses and alters sphingolipid composition

Received for publication, March 14, 2024, and in revised form, April 15, 2024 Published, Papers in Press, April 25, 2024,
https://doi.org/10.1016/j.jbc.2024.107320

Huaiyi Zhu, Yunfei You, Boming Yu, Zhitao Deng, Min Liu, Zhenying Hu, and Jingjing Duan*
From the Human Aging Research Institute and School of Life Sciences, Nanchang University, Nanchang, Jiangxi, China

Reviewed by members of the JBC Editorial Board. Edited by George M. Carman

Sphingolipids, essential membrane components and signaling molecules in cells, have ceramides at the core of their metabolic pathways. Initially termed as "longevity assurance genes", the encoding genes of ceramide synthases are closely associated with individual aging and stress responses, although the mechanisms remain unclear. This study aims to explore the alterations and underlying mechanisms of three ceramide synthases, HYL-1, HYL-2, and LAGR-1, in the aging and stress responses of *Caenorhabditis elegans*. Our results showed the knockdown of HYL-1 extends the lifespan and enhance stress resistance in worms, whereas the loss of HYL-2 function significantly impairs tolerances to heat, oxidation, and ultraviolet stress. Stress intolerance induced by HYL-2 deficiency may result from intracellular mitochondrial dysfunction, accumulation of reactive oxygen species, and abnormal nuclear translocation of DAF-16 under stress conditions. Loss of HYL-2 led to a significant reduction of predominant ceramides (d17:1/C20∼C23) as well as corresponding complex sphingolipids. Furthermore, the *N*-acyl chain length composition of sphingolipids underwent dramatic modifications, characterized by a decrease in C22 sphingolipids and an increase in C24 sphingolipids. Extra d18:1-ceramides resulted in diminished stress resilience in wild-type worms, while supplementation of d18:1/C16 ceramide to HYL-2-deficient worms marginally improved stress tolerance to heat and oxidation. These findings indicate the importance of appropriate ceramide content and composition in maintaining subcellular homeostasis and nuclear-cytoplasmic signal transduction during healthy aging and stress responses.

Ceramide, as a central intermediate of sphingolipid metabolism, not only acts as the skeleton for sphingomyelins and glycosphingolipids but also plays critical roles in cell death, autophagy, and various cellular stress responses (1, 2). *De novo* biosynthesis of ceramide is catalyzed by ceramide synthases (CerS) (3–5). The significance of CerS was identified as early as 30 years ago (6). The gene responsible for CerS expression in yeast is the so-called longevity assurance gene (*LAG1*), which is the first aging-related gene identified in *Saccharomyces cerevisiae*. *LAG1* expression decreases as yeast cells age and the deletion of *LAG1* results in a 50% increase in the lifespan of the mutated yeast (6). While depletion of another CerS in yeast, a homolog of the longevity assurance gene (*LAC1*), does not have a lifespan increase effect (7). LAC1 preferentially catalyzes the formation of dihydroceramides, while LAG1 tends to catalyze the formation of phytoceramides, which are specifically required for the establishment of a diffusion barrier against the proliferation of aging factors to daughter cells (8). These distinct substrate affinities and the specific effect of LAG1 on asymmetrical inheritance contribute together to induce different roles in cell aging.

Ceramides with distinct *N*-acyl chains have different roles in cellular physiology, and this view has been validated in higher organisms. In mammals, six paralogs of LAG1 have been identified and named CerS1-6 (3, 9–13). CerS1-6 exhibits distinct specificity toward substrates, which is determined by the length of the *N*-acyl chain (commonly C14-C26), as well as the degree of saturation and hydroxylation (14, 15). Sphingolipids with varying amide-linked fatty acid chain lengths exhibit differences in their tissue distribution (3, 16). Intriguingly, besides the differences in tissue expression and chain length specificity of ceramides, the subcellular distribution of these products may also contribute to the bio-functional specificity of CerS. While CerS5 and CerS6 exhibit similar substrate preferences, it is noteworthy that CerS6 but not the CerS5-derived C16:0 sphingolipids interacted with mitochondrial fission factor protein, leading to increased mitochondrial fragmentation and the development of insulin resistance and obesity (17).

Caenorhabditis elegans (*C. elegans*) is an exceptional organism for evaluating the bio-function of sphingolipids for lifespan, cellular supervision, and impairment repair and adapting to environmental stress (18). HYL-1 (named as the homolog of yeast longevity gene), HYL-2, and LAGR-1 are three CerS in *C. elegans* (19). CerS plays an essential for physiological activities in *C. elegans*, exhibiting notable distinctions (20–22). A high glucose diet caused mitochondrial dysfunction accompanied by reduced levels of *hyl-1* and *hyl-2* mRNA levels (23). HYL-2 plays a role in resisting anoxia stress (24), whereas the ceramide catalyzed by LAGR-1 functions as an indispensable second messenger in the radiation-induced

* For correspondence: Jingjing Duan, duan.jingjing@ncu.edu.cn.

apoptosis of germ cells (25). Supplementation with C24 ceramide can rescue the insufficiency of mitochondrial surveillance caused by the deficiency of sphingolipid levels (26). Loss-of-function mutants of HYL-1 or LAGR-1, but not HYL-2, alleviate radiation-induced cell apoptosis in worms (27). Although it shortens survival during starvation-induced L1 diapause (28), the absence of LAGR-1 and HYL-1 in worms leads to reduced food intake but a longer autophagy-dependent lifespan. Despite previous valuable investigations revealing the distinct roles of CerS in aging and some stress tolerance, the underlying mechanism remains unclear.

Ceramides have been implicated in stress tolerance and aging process (29–31). HYL-1, HYL-2, and LAGR-1 are three ceramide synthases in *C. elegans* that are responsible for catalyzing the acylation of sphingoid bases to ceramides (19, 27, 32). Each ceramide synthase exhibits distinct physiological functions, while the underlying mechanisms still remain largely elusive (24, 33). In this study, we assessed the sphingolipid profiles of *C. elegans* with functional loss of three ceramide synthases, HYL-1, HYL-2, and LAGR-1, and investigated the impact of their function on aging and stress tolerances, including exposure to heat, oxidation, and UV radiation.

Results

HYL-2 is essential for normal life history traits and stress tolerances in C. elegans

Nematodes lacking HYL-1 exhibit resilience to anoxia and heat stressors, while the functional loss of HYL-2 results in anoxia hypersensitivity, lipid depletion, and a reduced lifespan (Table 1). To further understand ceramide synthases on development, survival, and stress tolerances in *C. elegans*, we initially assessed the survival of each ceramide synthase mutant worm strain: *hyl-1(ok976)*, *hyl-2(ok1776)*, and *lagr-1(gk331)*. The results showed that the loss of function in HYL-1 resulted in a slight but statistically significant increase in lifespan, however, the loss of function in HYL-2 resulted in a dramatically shorter lifespan, as well as smaller body size, a shorter life cycle, and decreased motor ability (Fig. 1, Table 2). In contrast, the loss of function in LAGR-1 did not affect the lifespan in nematodes, but a slight increase in body bends was observed. The survivals of *hyl-1(ok976)*, *hyl-2(ok1776)*, and *lagr-1(gk331)* under heat, oxidation, and UV stress were subsequently evaluated. The median and maximum survivals of *hyl-1(ok976)* and *hyl-2(ok1776)* exhibited opposite trends under stress conditions (Table 2), with *hyl-1(ok976)* worms showing enhanced survival but *hyl-2(ok1776)* worms displaying reduced survival, regardless of stress type (Fig. 1, *F–H*). No difference in survival was observed between *lagr-1(gk331)* and wild-type animals under heat, or UV stresses, but *lagr-1(gk331)* showed a shorter median survival (17 h *versus* 23 h) under oxidative stress (Fig. 1*G*, Table 2). The significantly reduced survival and abnormal phenotypes caused by HYL-2 mutation highlight its importance for stress tolerance and healthspan in *C. elegans*.

The functional loss of HYL-2 alters sphingolipid composition in C. elegans

The varying effects of the three ceramide synthases, HYL-1, HYL-2, and LAGR-1, on the healthy lifespan and stress tolerance in *C. elegans* can be attributed to their distinct tissue distributions and catalytic product specificity. Amino acid sequence alignment revealed that LAGR-1 exhibited even higher homology with human CerS1 compared to HYL-1 and HYL-2 (Fig. S1). LAGR-1 is likely expressed in the head and pharynx of *C. elegans*, similar to CerS1 in humans, while HYL-1 and HYL-2 may have a broader distribution. HYL-1 may be responsible for synthesizing ceramides with longer acyl chains, whereas HYL-2 catalyzes the synthesis of ceramides and sphingolipids containing shorter acyl-fatty acid side chains (24). However, the substrate preference of LAGR-1 remains unclear (Table 1). Our sphingolipidomics data revealed distinct clustering of sphingolipid profiles among wild-type and three CerS mutant worm stains (Fig. 2*A*). The functional loss of each ceramide synthase resulted in decreased levels of ceramides (Cer), hexosylceramide (HexCer), and sphingomyelins (SM), with the most significant decrease observed in *hyl-2(ok1766)* animals (Fig. 2*B*). Despite the low levels of 1-

Table 1
Stress response phenotypes, and majorly reduced ceramides of ceramide synthetase mutants

CerS	Phenotypes of the gene	Possible tissue expression[a]	Majorly reduced ceramides
HYL-1	Resistance to radiation-induced germ cell apoptosis (Deng X *et al.*, 2008) Lipid composition variant and autophagy (Mosbech MB *et al.*, 2013) Resistance to anoxia (Menuz *et al.*, 2009) Resistance to heat stress (Chan *et al.*, 2017; Fig. 1*F*) Resistance to oxidation stress (Fig. 1*G*) Resistance to UV stress (Fig. 1*H*)	Germ line, head mesodermal cell, intestine, neuron system, pharynx	C22-C24 (Menuz *et al.*, 2009) ≥C24 (Mosbech MB *et al.*, 2013) C16-18, ≥C24 (Fig. 2*D*)
HYL-2	Anoxia hypersensitive (Menuz *et al.*, 2009) Lipid composition variant (Mosbech MB *et al.*, 2013) Lipid depleted (Garcia AM *et al.*, 2015) Shortened life span (Mosbech MB *et al.*, 2013) Heat, oxidation, and UV stress hypersensitive (Fig. 1, *F–H*)	Head, hypodermis, intestine, tail, terminal bulb	C20-C22 (Menuz *et al.*, 2009) ≤C22 (Mosbech MB *et al.*, 2013) C20-C23 (Fig. 2*D*)
LAGR-1	lipid composition variant and autophagy (Mosbech MB *et al.*, 2013) oxidation stress hypersensitive (Fig. 1*G*)	Pharynx	Subtle effects (Mosbech MB *et al.*, 2013, Fig. 2*D*)

[a] Data from wormbase.org.

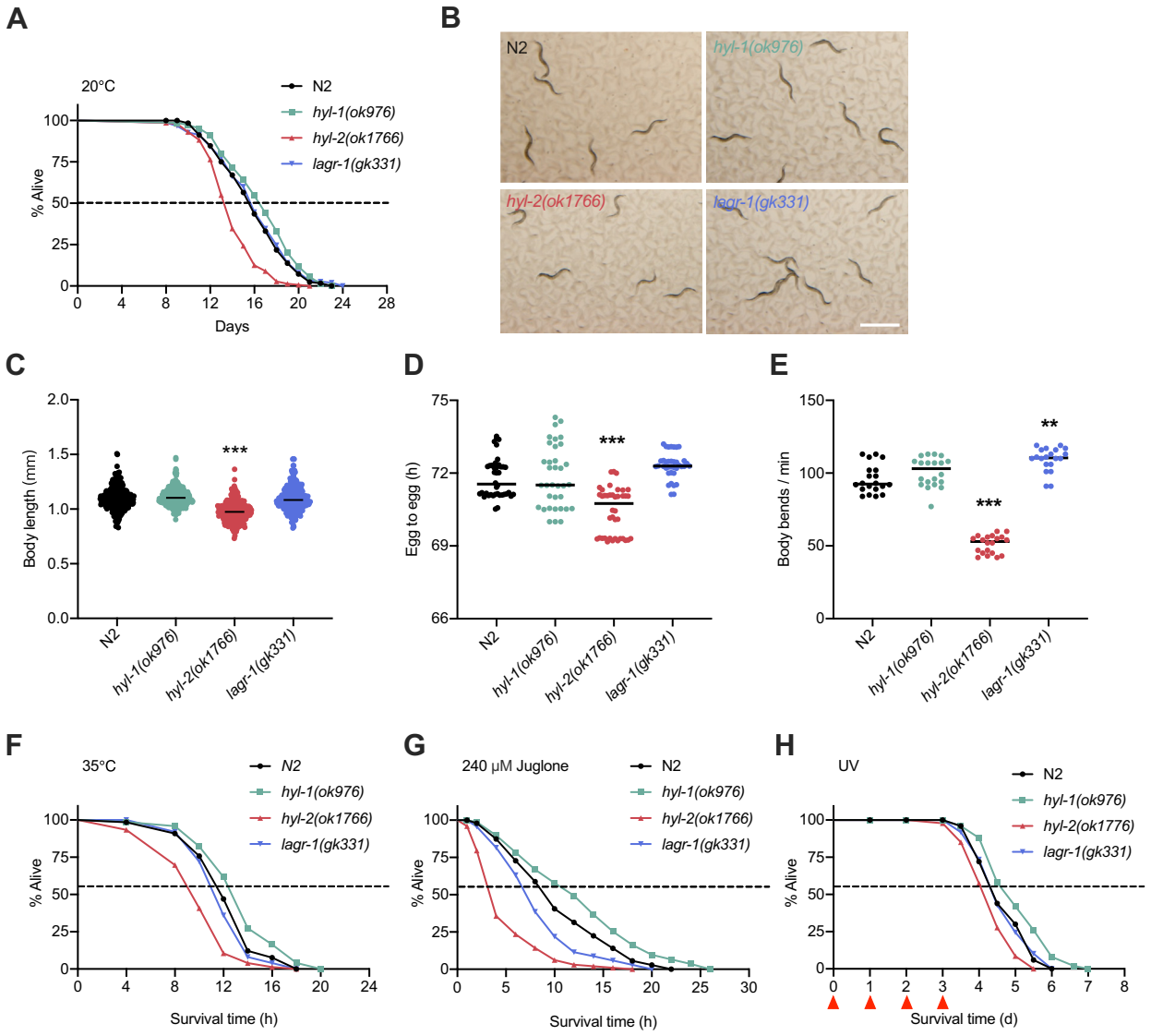

Figure 1. HYL-2 mutant reduces normal life history traits and stress tolerances in *C. elegans*. *A*, survival curves of wild-type (N2, n = 123) and ceramide synthase mutant animals, *hyl-1(ok976, n = 145)*, *hyl-2(ok1766, n = 144)*, and *lagr-1(gk331, n = 150)*, under standard culture conditions were plotted and analyzed. Days were counted from egg lay as day 0 for all animals (*abscissa*). *B*, images of WT and ceramide synthase mutation animals at the day 4 stage captured using a Nikon optical microscope. Scale bar, 1 mm. *C*, the body lengths of day 4 animals were measured under a microscope and statical analyzed. n > 200. *D*, the duration from a fresh egg (F1) to the first egg (F2) laid by each hatched nematode (F1) was monitored under normal culture conditions. *E*, day 7 nematodes were placed in M9 buffer and counted for their total body bends in 1 min. Results are presented as mean values. The *p* values are relative to WT (N2) animals analyzed by two-tailed student's *t* test (**$p < 0.01$; ***$p < 0.001$). *F*, day 7-stage wild-type (N2, n = 66), *hyl-1(ok976, n = 73)*, *hyl-2(ok1766, n = 76)*, and *lagr-1(gk331, n = 75)* nematodes were subjected to survival analysis in a 35 °C incubator. *G*, survival of Day 7-stage wild-type (N2, n = 143), *hyl-1(ok976, n = 166)*, *hyl-2(ok1766, n = 98)*, and *lagr-1(gk331, n = 113)* nematodes were monitored under oxidative stress induced by 240 μM juglone. *H*, the survival of wild-type (N2, n = 50), *hyl-1(ok976, n = 50)*, *hyl-2(ok1766, n = 47)*, and *lagr-1(gk331, n = 49)* animals was assessed after exposure to four rounds of UV radiation from the day 7 stage.

Table 2
Survival of ceramide synthase mutants in *Caenorhabditis elegans* in normal and stress conditions

	Normal condition			Heat stress			Oxidation stress			UV stress		
Survival	Median	Max		Median	Max		Median	Max		Median	Max	
Strains	Days			Hours			Hours			Days		
wild type (N2)	16 ± 0.27	23	n = 123	12 ± 0.33	18	n = 66	10 ± 0.41	22	n = 143	4.5 ± 0.13	6.0	n = 50
hyl-1(ok976)	17 ± 0.26	24	n = 145	14 ± 0.35*	20	n = 73	12 ± 0.47*	26	n = 166	5.0 ± 0.12*	7.0	n = 50
hyl-2(ok1766)	14 ± 0.19*	21	n = 144	10 ± 0.31*	18	n = 76	4 ± 0.33*	18	n = 98	4.0 ± 0.09*	5.5	n = 47
lagr-1(gk331)	16 ± 0.27	23	n = 150	12 ± 0.28	18	n = 75	8 ± 0.38*	20	n = 113	4.5 ± 0.10	6.0	n = 49

The heat stress: 35 °C exposure; Oxidation stress: 240 μM juglone treatment; UV stress: UV radiation at 0.1 J/cm^2 every 24 h for 4 times.
Statistical analysis was performed within the same data set, wild type(N2) was used as a control, significances were analyzed using the log-rank (Mantel-Cox) method and calculated against control (*$p < 0.001$). Median lifespan were presented as the mean ± standard error of mean (SEM).

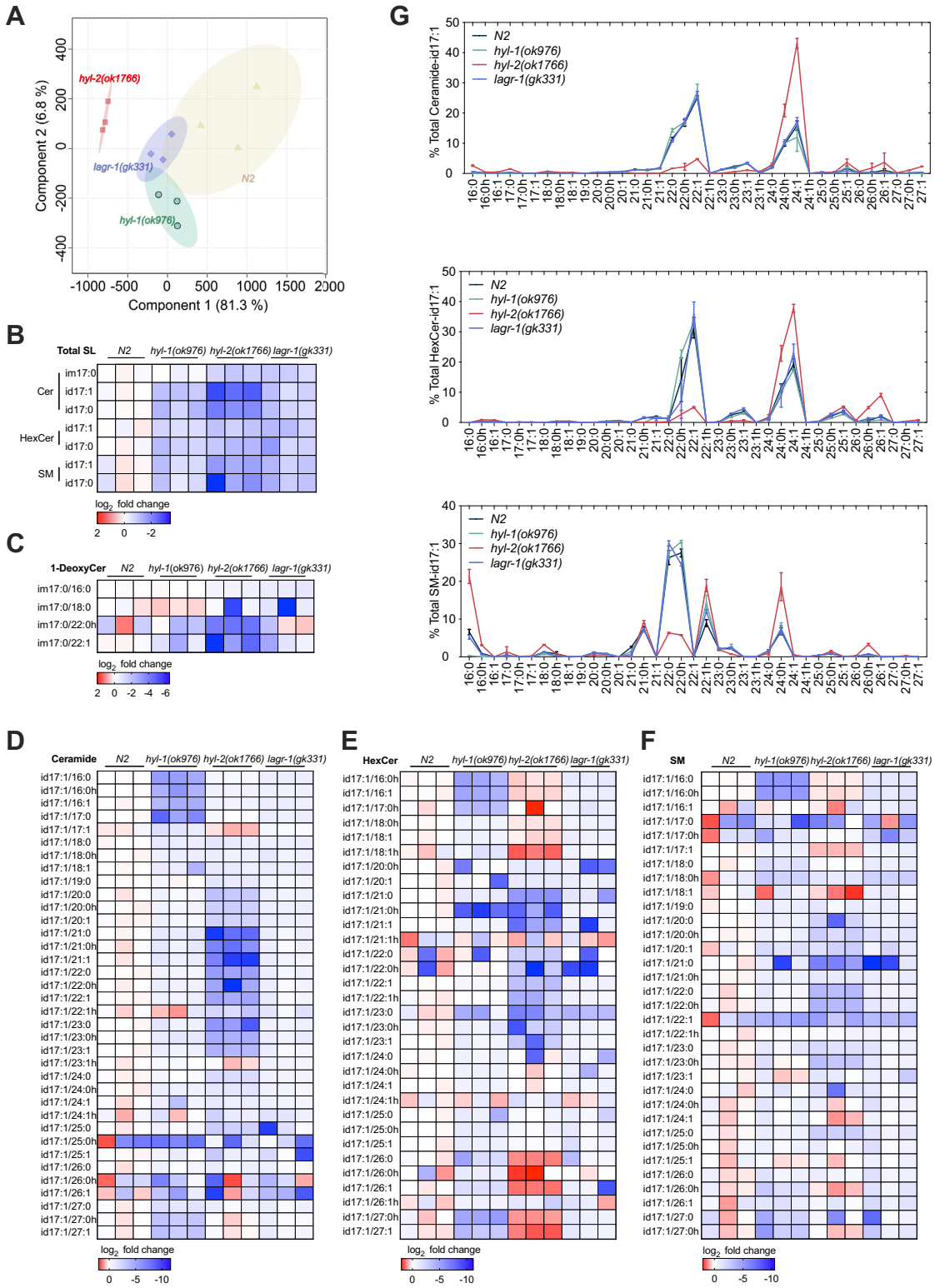

Figure 2. Sphingolipidomic analysis reveals the significant alteration in sphingolipid composition caused by deletion of *hyl-2*. *A*, partial least *squares* discriminant analysis (PLS-DA) of quantified SLs shows separation of N2 worms with the three CerS mutant strains. *B–F*, heatmap showing log2-fold change in the amount of sphingolipids species in the mutant strains compared with N2 worms (n = 3 per group). The *white* color is set as the average of all samples, with increasing *red* indicating higher lipid levels and increasing *blue* indicating lower levels. *B*, analysis of total levels of Cer, HexCer, and SM reveals a decrease in sphingolipid abundance in the posterior averages of *hyl-1*, *hyl-2*, and *lagr-1* knockouts with *hyl-2* deficiency showing the most pronounced reduction. *C*, decrease in the levels of atypical sphingolipids paticularly a significant reduction in C22 1-deoxyDHceramide in *hyl-2* deficiency. *D–F*, relative levels of Cer, HexCer, and SM with different *N*-acyl chain lengths. *D*, *hyl-1*, *hyl-2*, and *lagr-1* gene knockout samples show decreased ceramide levels, with *hyl-1* mutant exhibiting a significant reduction in ceramides with C16 to 18, ≥C24 acyl chain lengths. The *hyl-2* mutant demonstrated a pronounced decrease in ceramide levels with C20∼23 acyl chain lengths, while *lagr-1* mutant displayed a non-specific reduction in ceramide levels across various chain lengths. *E* and *F*, HexCer and SM also exhibit variations in levels dependent on the *N*-acyl chain length, similar to the dependency observed in ceramide. The relative levels of sphingomyelins were analyzed, revealing differences in abundance based on the length of the acyl chains. *G*, the percentage of subtypes of sphingolipids based on *N*-acyl chain length classification in sphingolipidomics.

deoxyDHCer, there was a significant decrease in these atypical sphingolipids in *hyl-2(ok1766)* as well, particularly m17:0/C22 h and/C22:1 (Fig. 2*C*). Furthermore, id17-ceramides with shorter chain lengths (C16-C18) and very long chains (≥C24) were diminished in *hyl-1(ok976)*, while ceramides with long chain fatty acids (C20∼C23) were significantly reduced in *hyl-2(ok1766)* worms. There was a relatively mild overall reduction in *lagr-1(gk331)* (Fig. 2*D*). These results were consistent across Cer, HexCer, SM, and their corresponding dihydro-molecules (Figs. 2, *D–F* and S2). These results demonstrate the chain-length substrate specificity of HYL-1 (involving shorter chain length, C16∼C18 and very long chains, ≥C24) and HYL-2 (involving long chain fatty acids, C20∼C23), with the latter synthesizing predominantly C20∼C23 ceramides (Fig. 2, *D* and *G*). Additionally, changes in the quantity of sphingolipids corresponded with significant alterations in the proportion of *N*-acyl chain length subtypes, underscoring their biological relevance. While N2, *hyl-1(ok976)*, and *lagr-1(gk331)* worms exhibited high consistency in sphingolipid composition, *hyl-2(ok1766)* worms displayed specific alterations, characterized by a decrease in the proportion of C22 sphingolipids and an increase in the proportion of C24 sphingolipids (Fig. 2*G*). This pattern was consistent across both ceramides and complex sphingolipids, suggesting an association between dysregulated subtype proportions and the impaired phenotype observed in *hyl-2(ok1766)* worms.

HYL-2 functional loss enhances ROS accumulation under stress

Heat and oxidative stress induce the generation of reactive oxygen species (ROS) in the cytoplasm and mitochondria, which correlats positively with lifespan-shortening in *C. elegans* (34). To understand the involvement of ceramide synthesis in stress tolerance, we assessed ROS levels in mutant worms on day 7, following exposure to heat or oxidative stress. Intracellular ROS levels were measured using a dichlorofluorescein-diacetate (DCFH-DA) assay, revealing excessive whole-body ROS accumulation in hyl-*2(ok1776)* animals under both 35 °C heat and 240 μM juglone-induced oxidative stress, compared to the N2 wild-type nematodes (Fig. 3*A*). To confirm that the elevated ROS levels were not limited to juglone-induced oxidative stress, *hyl-2(ok1776)* animals were subsequently treated with 40 mM H_2O_2, resulting in a similar pattern of elevated ROS levels (Fig. S3, *A* and *B*). While whole-body ROS slightly increased in *hyl-1(ok976)* under heat stress, there were no significant alterations in *lagr-1(gk331)* (Fig. 3*A*). Given that elevated ROS may predominantly be generated by mitochondria, mitochondrial ROS (mtROS) levels were further detected using MitoTracker Red CMXRos (Invitrogen). Results showed significantly higher mtROS levels in the *hyl-2 (ok1776)* strain compared to the wild-type and other strains (Fig. 3*B*). Furthermore, oxidative stress tolerance in *hyl-2 (ok1776)* significantly improved upon treatment with the ROS scavenger *N*-acetylcysteine (NAC) (Fig. S3*C*). These findings suggest that over-accumulation of mtROS may contribute to stress intolerance observed in *hyl-2 (ok1776)* worms.

Functional loss of HYL-2 exacerbates stress-induced mitochondria morphological alternations and dysfunction

The rise in ROS levels could be due to morphological and functional disorders of mitochondria. The assessment of mitochondrial morphology using MitoTracker deep red (MTDR) staining and a mitochondrial GFP reporter strain revealed that mitochondrial networks in *hyl-2(ok1766)* worms were less organized and more dispersed compared to those in wild-type worms (Fig. 3*C*). This observation was further confirmed through RNA interference (RNAi) experiments targeting HYL-1, HYL-2, and LAGR-1 in a transgenic strain *SJ4103[myo-3::GFP(mit)]* expressing GFP in body wall muscle cell mitochondria. To further investigate the role of HYL-2 in mitochondrial regulation, we measured mitochondrial copy numbers in N2 worms and ceramide synthase mutants. Our results showed that the loss of HYL-2 function led to a reduction in mitochondrial DNA (mtDNA) (Fig. 3*D*), suggesting a decrease in either the number of mitochondria per cell or the number of mitochondrial genomes per mitochondrion. This decline in mtDNA resulted in impaired mitochondrial function, as evidenced by a significant decrease in ATP levels in *hyl-2(ok1766)* worms compared to wild-type worms (Fig. 3*E*). The results demonstrated that HYL-2 deficiency impaired mitochondrial function and altered morphology, exacerbating mitochondrial dysfunction induced by heat stress or oxidative stress (Figs. 3, *F* and *G*, S4). These findings suggest a crucial role for HYL-2 played in maintaining mitochondrial morphology and function under stress conditions.

The regulation of mitochondrial morphology through fusion and fission processes was analyzed by evaluating the expression levels of related genes in mutant nematodes using qRT-PCR. The results revealed a suppression of the overall gene expression associated with mitochondrial fission and fusion in *hyl-2(ok1766)* worms compared to the N2 control group under normal, heat, and oxidative stress conditions, indicating weakened mitochondrial metabolism in *hyl-2(ok1766)* worms (Fig. S5). Conversely, an increased mRNA expression level in *hyl-1(ok976)* worms compared to the N2 control group under stress conditions suggests activation of mitochondrial quality control mechanisms. This observation may contribute to the hypothesis that improved mitochondrial morphology and function in HYL-1 mutants leads to higher survival rates, whereas the highly disordered mitochondria in HYL-2 functional loss animals result in shorter survival times and lower survival rate under stress conditions.

Functional loss of HYL-2 or LAGR-1 disrupts DAF-16 nuclear accumulation in response to stress

The forkhead transcription factor DAF-16, akin to the mammalian FoxO protein, plays a vital role in various stress response and aging processes (35, 36). Its activation is characterized by translocalization to the nucleus, as observed during heat stress (Fig. S6). To investigate the potential involvement of the DAF-16 signaling pathway in the reduced lifespan and stress intolerance associated with *hyl-2* mutation,

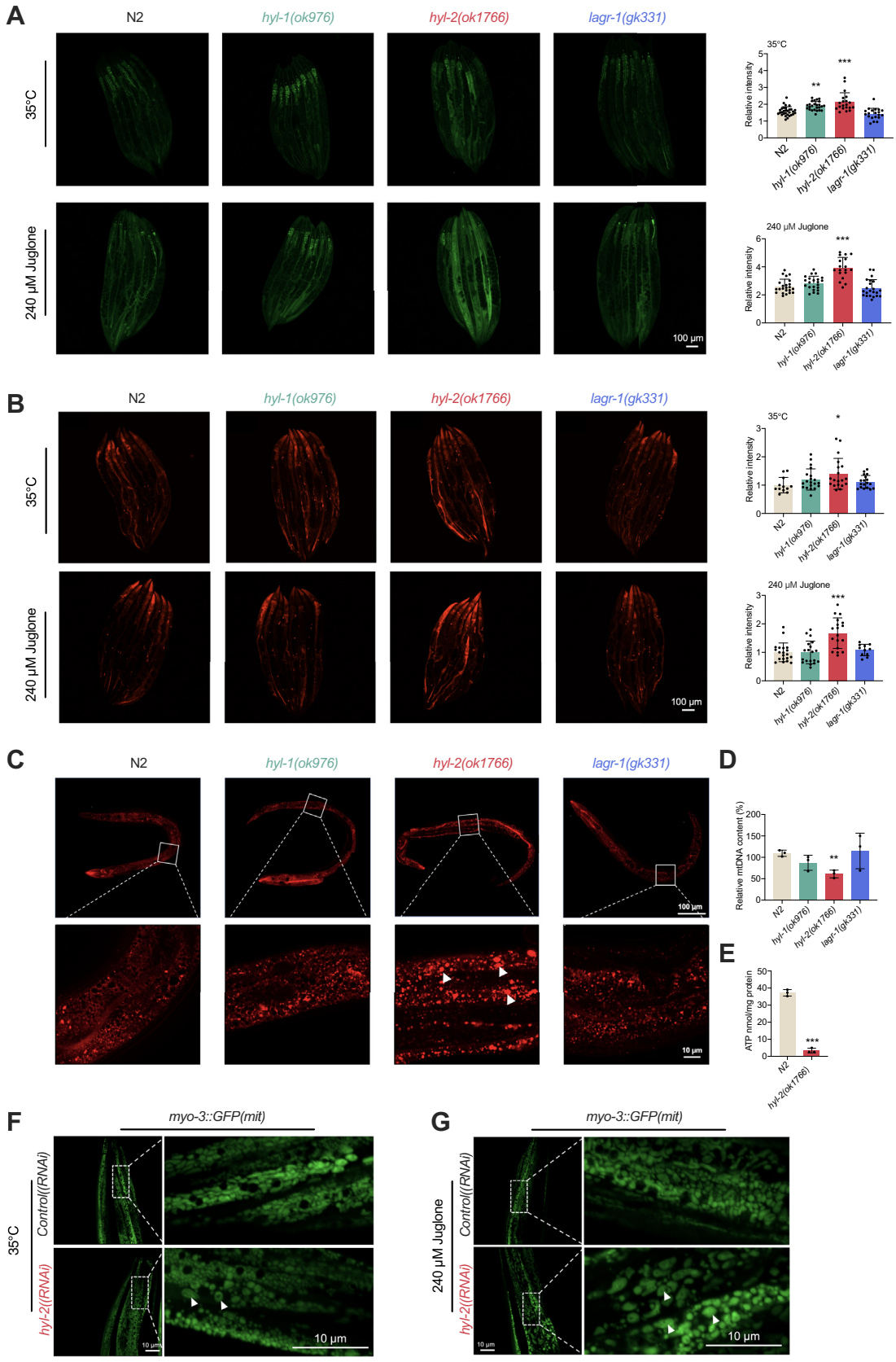

Figure 3. *Hyl-2* is required for maintaining ROS homeostasis under heat and oxidative stress. *A*, wild-type (N2) and ceramide synthase mutant nematodes were exposed to 35 °C heat or 240 μM juglone-induced oxidative stress. Intracellular ROS levels of worms were assessed by monitoring green fluorescence using dichlorofluorescein (DCF). Scale bar, 100 μm. *B*, mitochondrial ROS levels were determined by staining with MitoTracker Red CMXRos (MTRC), represented by red fluorescence. Scale bar, 100 μm. The rightmost graphs display the quantitative results for each condition. Error bars represent SD (two-tailed student's *t* test, $*p < 0.05$; $**p < 0.01$; $***p < 0.001$). *C*, fluorescence micrographs showed MitoTracker Deep Red (MTDR)-labeled

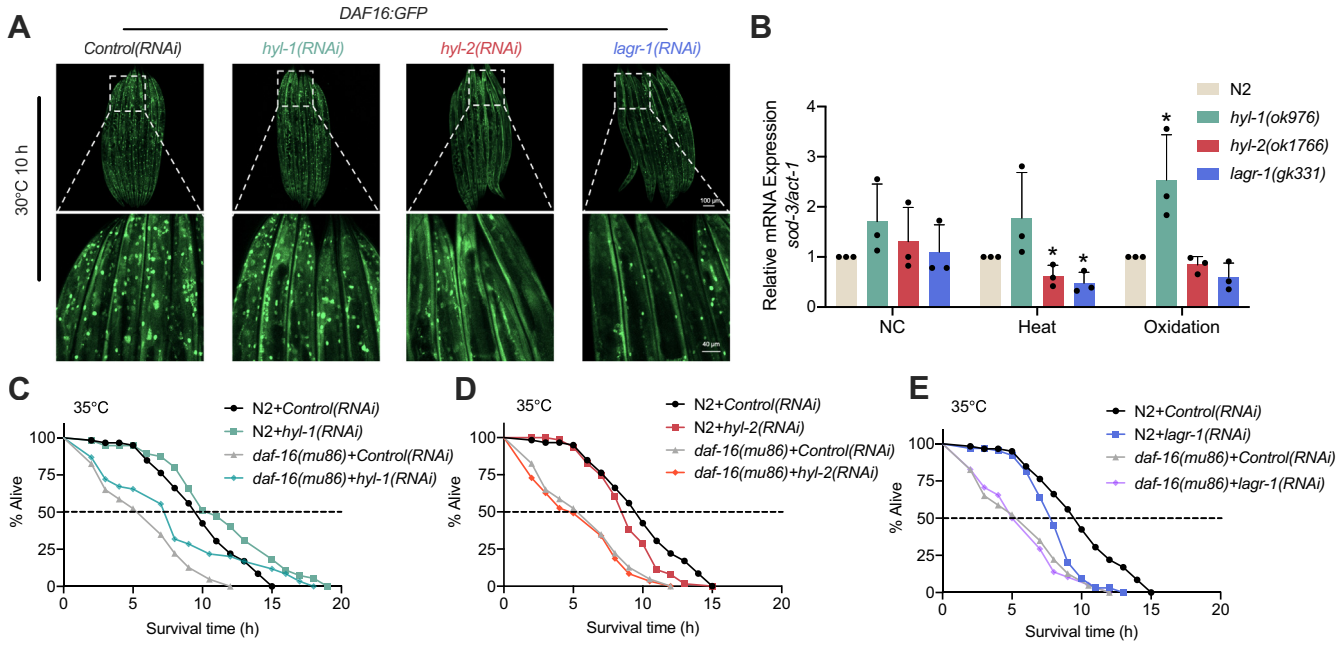

Figure 4. Functional loss of *hyl-2* or *lagr-1* disturbs DAF-16 nuclear accumulation in response to stress. *A*, mild heat stress (30 °C, 8 h) induced differential nuclear accumulation of DAF-16 in response to either empty vector control bacteria *Control(RNAi)* or the indicated RNAi strains. *hyl-2(RNAi)* and *lagr-1(RNAi)* led to reduced nuclear entry of DAF-16 under heat stress, while *hyl-1(RNAi)* showed similar effects to control bacteria. Scale bar of main image panel, 100 μm and associated zoom magnification image panel, 40 μm. *B*, quantitative RT-PCR (qRT-PCR) analysis of *sod-3* expression in wild-type (N2) and mutant nematodes at day 7 after heat stress (30 °C, 10 h) and oxidative stress (120 μM juglone, 10 h). Error bars represent SD (n = 3, two-tailed student's *t* test, $*p < 0.05$; $**p < 0.01$; $***p < 0.001$). *C–E*, cumulative survival curves of N2 and *daf-16(mu86)* under 35 °C heat stress, exposed to either empty vector control bacteria *Control(RNAi)* or the indicated RNAi strains. The heat stress response of the indicated RNAi strains mirrored the corresponding mutant lines. *C*, when subjected to *hyl-1(RNAi)*, the reduced lifespan of *daf-16(mu86)* was extended but not fully restored to the level of N2 animals. *D* and *E*, when subjected to *hyl-2(RNAi)* and *lagr-1(RNAi)*, the shortened lifespan of N2 did not appear in *daf-16(mu86)* animal.

we individually knocked down ceramide synthase genes using RNAi in a transgenic strain expressing DAF-16::GFP (*TJ356*). Imaging results showed that the nuclear translocalization of DAF-16 was impaired upon *hyl-2* or *lagr-1* RNAi under heat stress compared to *control(RNAi)*, while *hyl-1 RNAi* did not affect DAF-16 activation (Fig. 4*A*). Additionally, the mRNA expression of *sod-3*, a DAF-16 target gene encoding a protein that reduces intracellular superoxide radicals, was reduced in heat-stressed *hyl-2(ok1766)* and *lagr-1(gk331)* strains compared to control (Fig. 4*B*).

To explore the relationship between DAF-16 and ceramide synthase function, we employed RNA interference on a *daf-16(mu86)* strain and evaluated survival under heat stress. The survival rates of *hyl-1*, *hyl-2*, and *lagr-1* RNAi under 35 °C heat stress were similar to those of the mutant lines. Notably, *hyl-1* RNAi resulted in greater stress tolerance ($p < 0.001$, Fig. 4*C*), suggesting that the stress tolerance induced by *hyl-1* RNAi may occur independently of DAF-16. Conversely, neither *hyl-2* nor *lagr-1* RNAi exacerbated stress damage in *daf-16(mu86)* mutants under heat stress, as evidenced by overlapping survival curves ($p = 0.523$ and $p = 0.708$, respectively, Fig. 4, *D* and *E*). These findings support the observations of DAF-16 nucleus localization and *sod-3* qRT-PCR results, emphasizing the involvement of DAF-16 in the abnormal stress tolerance of *hyl-2(ok1766)* and *lagr-1(gk331)* nematodes.

Supplementation of d18:1/C16 ceramide marginally rescued stress resilience in hyl-2 *mutants*

The supplementation of d18:1- ceramides with varying chain lengths (C16, C20, C22, and C24) to wild-type worms (N2) appeared to exacerbate heat or oxidative stress-induced reduction in survival rates, resulting in increased ROS levels in the nematodes (Fig. S7). Subsequently, we supplemented *hyl-2(ok766)* worms with these ceramides to assess their potential to mitigate or exacerbate the detrimental phenotype caused by ceramide synthase deficiency. Supplementation with d18:1/C24 ceramide further intensified ROS accumulation and worsened oxidative stress tolerance in *hyl-2(ok766)* worms (Fig. S8, *A* and *B*). In contrast, supplementation with d18:1/C16 ceramide demonstrated a modest rescue effect on stress tolerance and the expression levels of mitochondrial fission-fusion-related genes (Fig. 5, *A–D*). While supplementation with d18:1-ceramides failed to rescue mitochondrial morphological disorder or decreased nuclear localization of DAF16 of *hyl-2(ok1766)* with a

mitochondria in wild-type (N2) and mutant nematodes, with a higher magnification image of the mitochondria. *D*, compared to wild-type worms (N2), *hyl-2(ok1766)* worms exhibited a lower mitochondrial copy number at day 7 of adulthood. *E*, ATP production was reduced in *hyl-2(ok1766)* worms at day 7 of adulthood compared to wild-type worms (N2). Scale bar of main image panel, 100 μm and associated zoom magnification image panel, 10 μm. Error bars represent SD (n = 3, two-tailed student's *t* test, $*p < 0.05$; $**p < 0.01$; $***p < 0.001$). *F* and *G*, comparison of body wall muscle mitochondrial between *hyl-2(RNAi)*-treated and *Control(RNAi)*-treated SJ4103 strain worms at day 7 under 35 °C heat or 240 μM juglone-induced oxidation stress, using a mitochondrially localized GFP reporter. The *white arrow* indicates abnormal mitochondrial morphology, Scale bar, 10 μm.

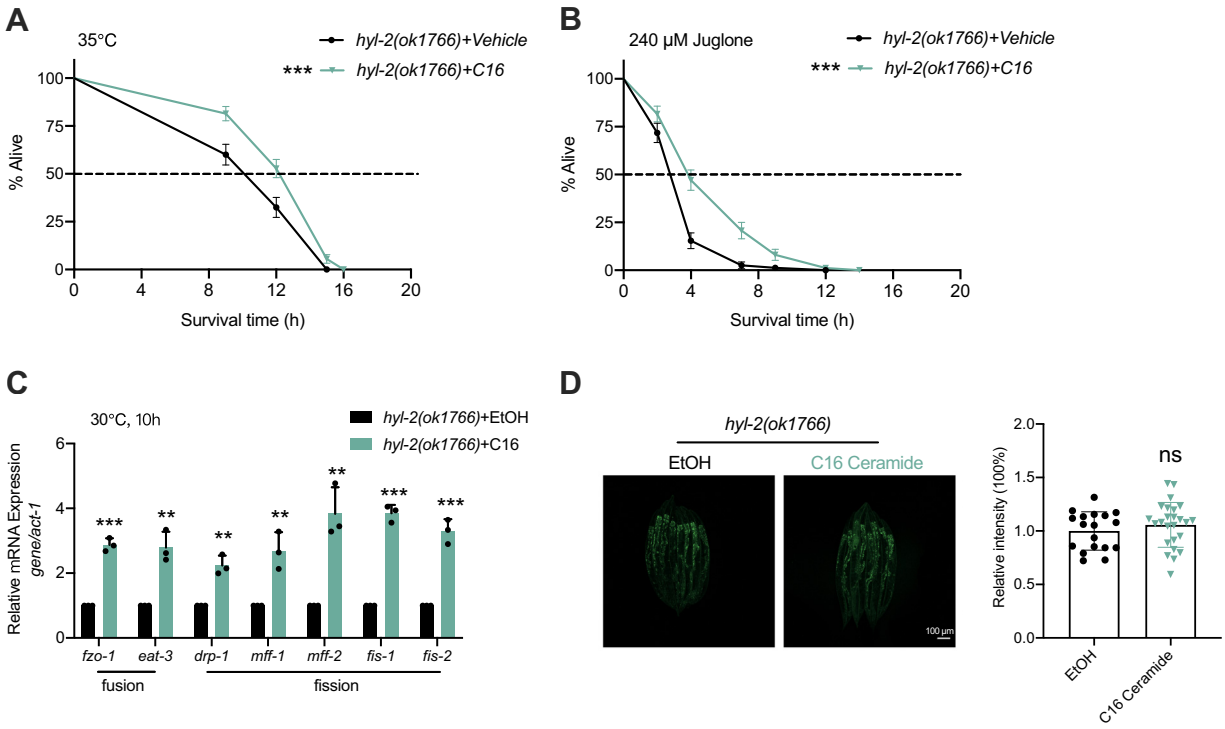

Figure 5. Exogenous supplementation of C16 ceramide marginally rescues the decrease in stress tolerance caused by HYL-2 dysfunction. *A* and *B*, supplementation of d18:1/C16 ceramide in HYL-2-deficient worms marginally rescued their stress tolerance and the expression of mitochondrial fission and fusion genes (*C*). *D*, this supplementation did not lead to further accumulation of reactive oxygen species (ROS).

diminished corresponding chain length of id17-ceramides (Fig. S8, *C* and *D*).

Discussion

In the current study, we aimed to characterize the involvement of three ceramide synthases (HYL-1, HYL-2, and LAGR-1) in the defense mechanism of *C. elegans* against heat stress (35 °C) and oxidative stress induced by juglone. Our findings revealed that while HYL-1 loss function improves the nematode survival under normal and stress conditions, HYL-2 is essential for normal life history traits and stress tolerance in *C. elegans* (Table S1). Interestingly, *hyl-2* mutants were significantly smaller, which may be attributed to mitochondrial dysfunction-mediated energy deficiency or the effects of *hyl-2* on growth factors. LGAR-1 results in mild damage under heat and oxidative stresses, possibly due to its limited tissue distribution and substrate preference (27, 33). These results partially align with prior studies (24, 33), indicating that HYL-1 and HYL-2 have opposing effects on aging: loss of HYL-1 is beneficial, whereas loss of HYL-2 decreases lifespan and stress tolerance (Table 2).

The disparity may be due to different roles in the synthesis of distinct chain lengths of ceramides and downstream complex sphingolipids. In N2 *C. elegans*, the predominant ceramides were id17:1/C20∼C23 synthesized by HYL-2, while HYL-1 was responsible for shorter (C16-C18) and very long-chain (≥C24) ceramides (Fig. 2). In *hyl-2(ok1766)* mutants, the content of 1-deoxyceramide containing C22 was reduced, indicating that m17:0/C22 ceramide could be synthesized by HYL-2 using m17:0 as substrate. It has been reported that shorter-chain ceramides can resist radiation-induced apoptosis, while long-chain ceramides can accelerate cancer cell death under chemotherapy (37). Our study demonstrates that excessive ceramide-induced ROS is considered harmful. Furthermore, supplementation of d18:1/C20∼C23 ceramides, corresponding to the *N*-acyl chain lacking in HYL-2 deficient worms, failed to alleviate stress intolerance phenotypes. Caution must be exercised when interpreting the effects of exogenous supplementation, as the endogenous sphingolipids of *C. elegans* are composed of iso-d17-sphingoid backbones, which differ structurally from supplemented mammalian sphingolipids (d18-). Nonetheless, supplementation of d18:1/C16, a ceramide with a shorter *N*-acyl chain, partially improved the adverse phenotype. This suggests that functional differences between long and short-chain sphingolipids also exist in *C. elegans*.

Glycosphingolipids and sphingomyelins are the main components of biofilms, and it has been hypothesized that complex sphingolipids with different amide chain lengths have distinct effects on physical properties, such as fluidity and permeability, of plasma and subcellular membranes (38). Therefore, the modification of ceramide synthase may induce biophysical and functional alternation of membranes. Ceramides have been reported to localize in the inner membrane of mitochondria to regulate mitochondrial autophagy under stress conditions (17). Our results demonstrate that the absence of ceramides with C20∼23 *N*-acyl fatty acids caused more pronounced disorders in mitochondrial morphology and function in nematodes under stress. Additionally, ceramide synthase deficiency affected

gene expressions of mitochondrial fusion and fission in *C. elegans*, the underlying mechanisms require further study. The absence of *hyl-2* and *lagr-1* affected the nuclear localization of DAF-16 and the expression of its downstream target gene *sod*-3. We hypothesize that different ceramides may also play a role in the heterogeneity of transcriptional regulation and post-transcriptional regulation of these genes.

One possible explanation for the observed phenomenon that "loss of HYL-1 appears to be beneficial, whereas the loss of HYL-2 is harmful to *C. elegans*" is that a moderate reduction in ceramide levels may confer benefits, while excessive reduction or inhibition of key ceramide types may be detrimenta. Another plausible interpretation is that certain types of sphingolipid species, such as id17:0/or id17:1/C20∼C23 ceramides and downstream complex sphingolipids synthesized through HYL-2, are critical for maintaining ROS homeostasis, mitochondrial morphology, and function as well as nuclear localization of forkhead transcription factor. The consequences of the LAGR-1 mutation are comparatively subtle but significantly affect the nuclear translocation of DAF-16 with heat.

Our findings underscore the essential role of HYL-2 in maintaining normal lifespan and oxidative, heat, and ultraviolet stress while indicating the potential of HYL-1 as a target in aging. Given the intricate physiological functions of ceramide synthases and the diversity of their products as well as downstream metabolites, further investigations are warranted to elucidate the specific mechanisms connecting ceramides to specific aspects of aging or stress with the development and validation of specific modulators for each ceramide synthase.

Experimental procedures

C. elegans *strains and maintenance*

C. elegans were cultured on a nematode growth media (NGM) agar plate with a lawn of *Escherichia coli* strain OP50 at 20 °C unless otherwise specified for stress experiments. The first day after egg hatching was scored as day 1 for all experiments. The wild-type animals were Bristol strain (N2). Mutant strains, including *RB1036[hyl-1(ok976)]*, *RB1498[hyl-2(ok1776)]*, *VC765[lagr-1(gk331)]*, and transgenic strains *SJ4103[myo-3::GFP(mit)]*, CF*1038[daf-16(mu86)]*, *TJ356 [daf-16p::daf-16a/b::GFP + rol-6(su1006)]* were purchased from the *C. elegans* Genetics Center (CGC, University of Minnesota). Genotyping of the three ceramide synthase mutants was performed using specific PCR primers (Table S2), and the presence of deletion mutations was confirmed by agarose gel electrophoresis (Fig. S3*D*).

RNA interference

RNAi constructs targeting *hyl-1* and *lagr-1* were obtained from the Open Biosystems ORF-RNAi library (39) and underwent sequence verification before experimentation. The RNAi strain of *hyl-2* was constructed by our research group, and the targeted sequence accounted for 42% of the total mRNA and 60% of the CDS sequence, and the knockdown efficiency met the requirements. Synchronized L4 stage *C. elegans* nematodes were utilized. RNAi-treated strains were fed with *E. coli* HT115 bacteria carrying an L4440 empty vector as the *Control (RNAi)* or a vector expressing double-stranded RNAi targeting each ceramide synthase, namely *hyl-1(RNAi)*, *hyl-2(RNAi)*, and *lagr-1(RNAi)*, respectively. The identity of the clones were confirmed through sequencing.

Lifespan assay

A lifespan assay was conducted following the protocol described in reference (40). To synchronize populations, gravid nematodes were subjected to bleaching, and the resulting eggs were collected in an M9 buffer at room temperature for overnight incubation with gentle rocking. Subsequently, L1-stage nematodes were transferred to the NGM plate seeded with *E. coli* OP50. 50 worms at day 7 were monitored at the specified time points and transferred to a new NGM plate each day until the last worm exhibited no response to mechanical stimulation, determined by prodding with a platinum wire, indicating death.

Body movement assay

The body movement assay was conducted following the procedure described in reference (41). Synchronized eggs were allowed to grow until the L4 stage before being transferred to NGM plates seeded with OP50 bacteria for 7 days. Subsequently, they were cultured in an S-complete medium, and body movement was assessed by observing the number of bends observed over a 1-min period. Each experiment was conducted in triplicate, with 10 nematodes per replicate.

Body length assay

Synchronized worms were grown on NGM plates seeded with OP50 bacteria until adulthood. Then their body lengths were measured at various stages using a stereomicroscope (Zeiss, Axio Zoom.V16) with Zen software.

Measurement of ROS in C. elegans

The ROS levels were quantified using DCFH-DA (HY-D0940, MedChemExpress, USA). Day 7 worms were incubated with 10 μM DCFH-DA at 20 °C for 30 min. Subsequently, the treated worms were observed by a fluorescence microscope (Zeiss, LSM800) to detect dichlorofluorescein (DCF). The fluorophore MitoTracker Red CMXRos (MTRC, Cell Signaling Technology, 9082S) was used to measure the relative mitochondrial ROS production (42). Treated worms were stained with 0.5 μM MTRC for 12 h before microscopy observations.

Mitochondrial morphology

Mitochondrial morphology was assessed in worms labeled by 0.5 μM MitoTracker Deep Red (Thermo Scientific, M22426) and RNAi-treated SJ4103 strains. Following stress stimulation, the animals were collected and washed three times with M9 buffer. The alive nematodes were then rapidly transferred to a 2% agarose-coated slide (about 1 mm thick).

The observations were conducted by a confocal microscope (Zeiss, LSM800). We conducted three independent experiments and integrated the analysis of image results, showcasing specific regions.

Mitochondrial DNA analysis

Mitochondrial DNA content was quantified using quantification polymerase chain reaction (qPCR). DNA was extracted from individual *C. elegans* and resuspended in 10 μl PCR buffer (10 mM Tris–HCl pH 8.5, 50 nM Mg^{2+}, KCl free) as the template for qPCR. The experiments were conducted in triplicate, with 95 bp target PCR product of the mito fragment using forward primer "-CACACCGGTGAGGTCTTTGGTTC-" and reverse primer "-TGTCCTCAAGGC TACCACCTTCTTCA-", as well as 225 bp target PCR product of the nuclear fragment using forward primer "-TCCCGTCTATTGCAGGTCTTT CCA-" and the reverse primer "-GACGCGCACGATATCT CGATTTTC-".

ATP levels measurement

ATP levels were quantified using a Chemiluminescence ATP Determination Kit (Beyotime, S0027). The supernatant from approximately 500 synchronized worms was applied to the ATP Determination Kit. The luminescence signal was normalized to protein content, which was measured using a Pierce BCA protein determination kit (Thermo Scientific, 23227). The experiments were carried out in triplicate.

Stress assays

Heat stress assay was performed by transferring day 7 adult worms grown on OP50-NGM plates to a temperature of 35 °C, with survival monitored every 2 h. Oxidative stress assay involved transferring day 7 adult worms to 240 μM juglone NGM plates with an OP50 bacterial lawn, with survival recorded hourly until all worms had died. Nematodes displaying internal hatching, crawling off, or bursting were excluded from the analysis.

UV stress assay involved irradiating day 7 adult worms on OP50-free NGM plates using a germicidal bulb (254 nm) at a dose of 0.1 J/cm^2 for four consecutive days using UV cross-linkers. After each irradiation, animals were transferred to OP50-seeded NGM plates, with survival monitored every 12 h to generate survival curves.

Translocation of DAF-16

The *TJ356* strain, carrying a *daf-16::GFP* fusion gene, was employed to investigate the nuclear translocation of DAF-16 and its downstream gene *sod-3*. L4 larvae of *TJ356* worms were transferred to NGM plates seeded with *E. coli* expressing dsRNA specific to *hyl-1(RNAi)*, *hyl-2(RNAi)*, *lagr-1(RNAi)*, or *Control(RNAi)* strain. DAF-16 nuclear translocation was induced by incubating *TJ356* worms at 35 °C for 30 min or 30 °C for 8 h for mild heat stress induction. Confocal laser scanning microscope (Zeiss, LSM800, Germany) was utilized to capture the GFP intensity and location of DAF-16.

Lipid extraction

Approximately 5000 nematodes from each experimental group were used for lipid extraction. The worm samples were initially freeze-dried overnight and then homogenized with 1 ml H_2O. Each homogenized solution (900 μl) was transferred to a new glass tube, to which 1 ml of methanol and 0.5 ml of chloroform were added. The mixture was vortexed for 1 min and incubated in a water bath at 48 °C for 24 h after adding internal standard (25 pmol #LM-6005, Avanti Ploar Lipids). Following cooling, 150 μl of 1 M KOH in methanol was added and the mixture was briefly sonicated and then incubated with shaking for 2 h at 37 °C. After cooling, neutralization was achieved by adding 6 μl of glacial acetic acid. Upon centrifugation, the lower layer (chloroform phase) was carefully collected. The upper layer and interface were subjected to re-extraction using 1 ml of $CHCl_3$ by centrifugation. Then, the combined chloroform phases were evaporated using a speed vacuum, being careful not to overheat. The extracted residues were dissolved in LC solvents for LC-MS/MS analysis. The remaining 100 μl was used for protein quantification to normalize the sphingolipid content as pmol/mg.

Sphingolipidomics

The sphingolipids separation and analysis followed the protocol adopted from the LIPID MAPS protocols (www.lipidmaps.org) and a published method for sphingolipidomic analysis of *C. elegans* (43), with slight modifications, utilizing an ultra-high performance liquid chromatography (UPLC) system (Shimadzu, JP) coupled with a Triple Quad 5500^+ QTRAP (AB Sciex). The UPLC system comprised a binary pump system (LC-30AD), a degasser (DGU-20A5), a temperature-controlled autosampler (SIL-30AC), a column oven (CTO-20AC), and a control unit (CBM-20A). The mass spectrometer was operated in positive electrospray mode coupled with multiple reaction monitoring (MRM) transitions of mass-to-charge ratio (m/z), as detailed in Table S4. The ion source (ESI) voltage was set at 4.5 kV, and the ion source temperature was 400 °C. The ion source gas half and curtain gas flows were 60 psi and 40 psi, respectively. Dwell time and inter-channel delay were set to 50 and 5 ms. MS system was controlled by Analyst 1.7.3 software (Applied Biosystems). For chromatographic separation, a C18 column (2.6 μm, 100 × 2.1 mm, 100 Å, Phenomenex) was used with a binary solvent system comprised of mobile phase A (methanol: water: acetonitrile = 1:1:1, 7 mM ammonium acetate) and mobile phase B (isopropanol, 7 mM ammonium acetate). Prior to sample injection, the column was equilibrated for 2 min with 50% mobile phase B. The gradient elution was as follows: 0-1 min, 50% B; 1 to 10 min, 50 to 90% B; 10 to 11 min, 90 to 98% B; 11 to 13 min, 98% B; 13 to 14 min, 98 to 50% B; 13 to 14 min, 50% B. The flow rate was set at 0.3 ml/min, with 2 μl sample injection. For each LC analysis, mixture of standards (C17-sphinganine, C17-sphingosine, C17-sphingosine-1-phosphate, C17-sphinganine-1-phosphate, C12-ceramide, C12-ceramide-1-phosphate, C12-SM, C12-glucosylceramide, C12-lactosyl (β)-ceramide (Avanti Polar Lipids) were analyzed at the beginning, middle, and end of the run. In addition, the LC solvent as blank was analyzed at

varying intervals throughout the run to assess for possible carryover. If carryover or shifts in the LC retention times for any of the analytes or standards were noticed, the column was cleaned before resuming the run. Data analysis including peak smoothing and integration of areas under the curves for each peak was performed by SCIX OS (Version.3.0.0.3339, Applied Biosystems). The semi-quantitation of individual metabolites was normalized with the respective internal standards, and calculated with the formula as follows. Analyte Conc. (nmol/L) in worm sample = Area (analyte MRM peak) × Standard Conc.(nmol/L)/Area (Standard MRM peak). Multivariate and univariate analyses and partial least squares-discriminate analysis (PLS-DA) were used to identify features that differed markedly between different experimental groups, and performed based on the concentrations of SLs (>50 variables) by MetaboAnalyst (44). In the heatmap, each group was standardized against the N2 (wild type) group's average to show the variations in individual lipids clearly. The proportional line graph emphasizes the proportion of individual sphingolipids relative to the total within each subclass.

Ceramides supplementation

The d18:1-ceramides purchased from Avanti polar lipids were used for supplementation. Synchronized L1 worms (100 animals per dish) were cultured on a 3.5 cm dish with 20 μg ceramide dissolved in ethanol (20 μl), along with 20 μl OP50 seeding. ROS levels and survival under stress were assayed after 3 days.

RNA isolation and qRT-PCR

The Total RNA of nematodes was extracted using RNAiso Plus reagent (Takara Bio, Japan). Amplification and quantification of PCR products were conducted using the SYBR Green Real-Time PCR Supermix (Mei5 Biotechnology) and the qTOWER^{3}G Real-Time PCR Detection System (Analytikjena). The transcriptional expression levels of the target genes were normalized to *act-1*, which served as the internal control. The primers utilized for qRT-PCR are listed in (Table S3).

Statistical analysis

Lifespan curves were compared using the Kaplan–Meier survival method and analyzed by log-rank test. All other data are presented as the mean ± standard deviation (SD) unless specifically indicated. Statistical analyses included two-tailed student's *t* test or one-way analysis of variance (ANOVA) ($^*p < 0.05$; $^{**}p < 0.01$; $^{***}p < 0.001$). All figures were created and data were analyzed using GraphPad Prism 8 (GraphPad Software) and Photoshop CS3.

Data availability

Data underlying this article are available in the article and in its supporting Information.

Supporting information—This article contains supporting information.

Acknowledgments—We extend our sincere appreciation to Dr Alfred H. Merrill (Georgia Institute of Technology) for his invaluable guidance on sphingolipidomics and technical support. Additionally, we are grateful to Dr Yang Xiang (Nanchang University), Dr Fei Chen (Nanchang University),and Dr Huanhu Zhu (Shanghai Tech University) for their generous assistance with the *C. elegans* strains. We thank Jinsong Li and Rumei Sun for their help with this experiment. We are very grateful to Dr George M. Carman and Dr Emily Ulrich for their invaluable contributions, and to the reviewers for their insightful suggestions, both of which have significantly enhanced the quality of this paper.

Author contributions—Y. Y., H. Z., Z. D., Z. H., and M. L. methodology; H. Z. writing–original draft; H. Z. and B. Y. visualization; H. Z. data curation; H. Z. conceptualization; Z. H. software. J. D. writing–review & editing, J. D. resources, J. D. project administration, J. D. funding acquisition, J. D. formal analysis, J. D. conceptualization.

Funding and additional information—This work was supported by funding from the National Natural Science Foundation of China (82171551 and 31971043) and Jiangxi Provincial Natural Science Foundation (20232ACB205002) to Jingjing Duan.

Conflict of interest—The authors declare no competing interests.

Abbreviations—The abbreviations used are: CerS, ceramide synthases; DCF, dichlorofluorescein; LAG1, longevity assurance gene; mtDNA, mitochondrial DNA; MTDR, MitoTracker deep red; ROS, reactive oxygen species.

References

1. Ohanian, J., and Ohanian, V. (2001) Sphingolipids in mammalian cell signalling. *Cell. Mol. Life Sci.* **58**, 2053–2068
2. Hannun, Y. A., and Obeid, L. M. (2018) Sphingolipids and their metabolism in physiology and disease. *Nat. Rev. Mol. Cell Biol.* **19**, 175–191
3. Zelnik, I. D., Rozman, B., Rosenfeld-Gur, E., Ben-Dor, S., and Futerman, A. H. (2019) A Stroll down the CerS Lane. *Adv. Exp. Med. Biol.* **1159**, 49–63
4. Hannun, Y. A., and Obeid, L. M. (1995) Ceramide: an intracellular signal for apoptosis. *Trends Biochem. Sci.* **20**, 73–77
5. Kolesnick, R. N., and Krönke, M. (1998) Regulation of ceramide production and apoptosis. *Annu. Rev. Physiol.* **60**, 643–665
6. D'Mello, N.,P., Childress, A. M., Franklin, D. S., Kale, S. P., Pinswasdi, C., and Jazwinski, S. M. (1994) Cloning and characterization of LAG1, a longevity-assurance gene in yeast. *J. Biol. Chem.* **269**, 15451–15459
7. Jiang, J. C., Kirchman, P. A., Allen, M., and Jazwinski, S. M. (2004) Suppressor analysis points to the subtle role of the LAG1 ceramide synthase gene in determining yeast longevity. *Exp. Gerontol.* **39**, 999–1009
8. Megyeri, M., Prasad, R., Volpert, G., Sliwa-Gonzalez, A., Haribowo, A. G., Aguilera-Romero, A., *et al.* (2019) Yeast ceramide synthases, Lag1 and Lac1, have distinct substrate specificity. *J. Cell Sci.* **132**, jcs228411
9. Venkataraman, K., Riebeling, C., Bodennec, J., Riezman, H., Allegood, J. C., Sullards, M. C., *et al.* (2002) Upstream of growth and differentiation factor 1 (uog1), a mammalian homolog of the yeast longevity assurance gene 1 (LAG1), regulates N-stearoyl-sphinganine (C18-(dihydro)ceramide) synthesis in a fumonisin B1-independent manner in mammalian cells. *J. Biol. Chem.* **277**, 35642–35649
10. Riebeling, C., Allegood, J. C., Wang, E., Merrill, A. H., Jr., and Futerman, A. H. (2003) Two mammalian longevity assurance gene (LAG1) family members, trh1 and trh4, regulate dihydroceramide synthesis using different fatty acyl-CoA donors. *J. Biol. Chem.* **278**, 43452–43459
11. Lahiri, S., and Futerman, A. H. (2005) LASS5 is a bona fide dihydroceramide synthase that selectively utilizes palmitoyl-CoA as acyl donor. *J. Biol. Chem.* **280**, 33735–33738

12. Weinmann, A., Galle, P. R., and Teufel, A. (2005) LASS6, an additional member of the longevity assurance gene family. *Int. J. Mol. Med.* **16**, 905–910
13. Mizutani, Y., Kihara, A., and Igarashi, Y. (2006) LASS3 (longevity assurance homologue 3) is a mainly testis-specific (dihydro)ceramide synthase with relatively broad substrate specificity. *Biochem. J.* **398**, 531–538
14. Tidhar, R., and Futerman, A. H. (2013) The complexity of sphingolipid biosynthesis in the endoplasmic reticulum. *Biochim. Biophys. Acta* **1833**, 2511–2518
15. Wegner, M. S., Schiffmann, S., Parnham, M. J., Geisslinger, G., and Grösch, S. (2016) The enigma of ceramide synthase regulation in mammalian cells. *Prog. Lipid Res.* **63**, 93–119
16. Green, C. D., Maceyka, M., Cowart, L. A., and Spiegel, S. (2021) Sphingolipids in metabolic disease: the good, the bad, and the unknown. *Cell Metab.* **33**, 1293–1306
17. Hammerschmidt, P., Ostkotte, D., Nolte, H., Gerl, M. J., Jais, A., Brunner, H. L., *et al.* (2019) CerS6-Derived sphingolipids Interact with Mff and Promote mitochondrial fragmentation in obesity. *Cell* **177**, 1536–1552. e1523
18. Deng, X., and Kolesnick, R. (2015) *Caenorhabditis elegans* as a model to study sphingolipid signaling. *Biol. Chem.* **396**, 767–773
19. Jiang, J. C., Kirchman, P. A., Zagulski, M., Hunt, J., and Jazwinski, S. M. (1998) Homologs of the yeast longevity gene LAG1 in *Caenorhabditis elegans* and human. *Genome Res.* **8**, 1259–1272
20. Chan, J. P., Brown, J., Hark, B., Nolan, A., Servello, D., Hrobuchak, H., *et al.* (2017) Loss of sphingosine Kinase alters life history traits and Locomotor function in *Caenorhabditis elegans*. *Front. Genet.* **8**, 132
21. Haimovitz-Friedman, A., Kolesnick, R. N., and Fuks, Z. (1997) Ceramide signaling in apoptosis. *Br. Med. Bull.* **53**, 539–553
22. Cohen, L. B., and Troemel, E. R. (2015) Microbial pathogenesis and host defense in the nematode C. elegans. *Curr. Opin. Microbiol.* **23**, 94–101
23. Alcántar-Fernández, J., González-Maciel, A., Reynoso-Robles, R., Pérez Andrade, M. E., Hernández-Vázquez, A. J., Velázquez-Arellano, A., *et al.* (2019) High-glucose diets induce mitochondrial dysfunction in *Caenorhabditis elegans*. *PLoS One* **14**, e0226652
24. Menuz, V., Howell, K. S., Gentina, S., Epstein, S., Riezman, I., Fornallaz-Mulhauser, M., *et al.* (2009) Protection of *C. elegans* from anoxia by HYL-2 ceramide synthase. *Science* **324**, 381–384
25. Yang, Y., Xu, G., Xu, Y., Cheng, X., Xu, S., Chen, S., *et al.* (2021) Ceramide mediates radiation-induced germ cell apoptosis via regulating mitochondria function and MAPK factors in *Caenorhabditis elegans*. *Ecotoxicol. Environ. Saf.* **208**, 111579
26. Liu, Y., Samuel, B. S., Breen, P. C., and Ruvkun, G. (2014) *Caenorhabditis elegans* pathways that surveil and defend mitochondria. *Nature* **508**, 406–410
27. Deng, X., Yin, X., Allan, R., Lu, D. D., Maurer, C. W., Haimovitz-Friedman, A., *et al.* (2008) Ceramide biogenesis is required for radiation-induced apoptosis in the germ line of C. elegans. *Science* **322**, 110–115
28. Cui, M., Wang, Y., Cavaleri, J., Kelson, T., Teng, Y., and Han, M. (2017) Starvation-induced stress response is critically impacted by ceramide levels in *Caenorhabditis elegans*. *Genetics* **205**, 775–785
29. Zigdon, H., Kogot-Levin, A., Park, J. W., Goldschmidt, R., Kelly, S., Merrill, A. H., Jr., *et al.* (2013) Ablation of ceramide synthase 2 causes chronic oxidative stress due to disruption of the mitochondrial respiratory chain. *J. Biol. Chem.* **288**, 4947–4956
30. Volpert, G., Ben-Dor, S., Tarcic, O., Duan, J., Saada, A., Merrill, A. H., Jr., *et al.* (2017) Oxidative stress elicited by modifying the ceramide acyl chain length reduces the rate of clathrin-mediated endocytosis. *J. Cell Sci.* **130**, 1486–1493
31. Rao, R. P., Yuan, C., Allegood, J. C., Rawat, S. S., Edwards, M. B., Wang, X., *et al.* (2007) Ceramide transfer protein function is essential for normal oxidative stress response and lifespan. *Proc. Natl. Acad. Sci. U. S. A.* **104**, 11364–11369
32. Tedesco, P., Jiang, J., Wang, J., Jazwinski, S. M., and Johnson, T. E. (2008) Genetic analysis of hyl-1, the *C. elegans* homolog of LAG1/LASS1. *Age (Dordr)* **30**, 43–52
33. Mosbech, M. B., Kruse, R., Harvald, E. B., Olsen, A. S., Gallego, S. F., Hannibal-Bach, H. K., *et al.* (2013) Functional loss of two ceramide synthases elicits autophagy-dependent lifespan extension in *C. elegans*. *PLoS One* **8**, e70087
34. Dilberger, B., Baumanns, S., Schmitt, F., Schmiedl, T., Hardt, M., Wenzel, U., *et al.* (2019) Mitochondrial oxidative stress impairs energy metabolism and reduces stress resistance and longevity of *C. elegans*. *Oxid. Med. Cell. Longev.* **2019**, 6840540
35. Klotz, L. O., Sánchez-Ramos, C., Prieto-Arroyo, I., Urbánek, P., Steinbrenner, H., and Monsalve, M. (2015) Redox regulation of FoxO transcription factors. *Redox Biol.* **6**, 51–72
36. Lee, S. S., Kennedy, S., Tolonen, A. C., and Ruvkun, G. (2003) DAF-16 target genes that control *C. elegans* life-span and metabolism. *Science* **300**, 644–647
37. Fillet, M., Bentires-Alj, M., Deregowski, V., Greimers, R., Gielen, J., Piette, J., *et al.* (2003) Mechanisms involved in exogenous C2- and C6-ceramide-induced cancer cell toxicity. *Biochem. Pharmacol.* **65**, 1633–1642
38. Fabri, J., de Sá, N. P., Malavazi, I., and Del Poeta, M. (2020) The dynamics and role of sphingolipids in eukaryotic organisms upon thermal adaptation. *Prog. Lipid Res.* **80**, 101063
39. Rual, J. F., Ceron, J., Koreth, J., Hao, T., Nicot, A. S., Hirozane-Kishikawa, T., *et al.* (2004) Toward improving *Caenorhabditis elegans* phenome mapping with an ORFeome-based RNAi library. *Genome Res.* **14**, 2162–2168
40. Frakes, A. E., Metcalf, M. G., Tronnes, S. U., Bar-Ziv, R., Durieux, J., Gildea, H. K., *et al.* (2020) Four glial cells regulate ER stress resistance and longevity via neuropeptide signaling in *C. elegans*. *Science* **367**, 436–440
41. D'Amico, D., Mottis, A., Potenza, F., Sorrentino, V., Li, H., Romani, M., *et al.* (2019) The RNA-Binding protein PUM2 impairs mitochondrial dynamics and mitophagy during aging. *Mol Cell* **73**, 775–787.e710
42. Lu, X., Xuan, W., Li, J., Yao, H., Huang, C., and Li, J. (2021) AMPK protects against alcohol-induced liver injury through UQCRC2 to up-regulate mitophagy. *Autophagy* **17**, 3622–3643
43. Cheng, X., Jiang, X., Tam, K. Y., Li, G., Zheng, J., and Zhang, H. (2019) Sphingolipidomic analysis of *C. elegans* reveals development- and Environment-dependent metabolic features. *Int. J. Biol. Sci.* **15**, 2897–2910
44. Lu, Y., Pang, Z., and Xia, J. (2023) Comprehensive investigation of pathway enrichment methods for functional interpretation of LC-MS global metabolomics data. *Brief. Bioinform.* **24**, bbac553